A global-local approach for the elastoplastic analysis of compact and thin-walled structures via refined models

A global-local approach for the elastoplastic analysis of compact and thin-walled structures via refined models

M. Petrolo*, M.H. Nagaraj†, I. Kaleel‡, E. Carrera§
MUL^2 Group, Department of Mechanical and Aerospace Engineering,
Politecnico di Torino, Corso Duca degli Abruzzi 24, 10129 Torino, Italy

Revised version of manuscript number CAS_2018_108

Author for correspondence:
M. Petrolo, Assistant Professor,
MUL^2 Group, Department of Mechanical and Aerospace Engineering,
Politecnico di Torino,
Corso Duca degli Abruzzi 24,
10129 Torino, Italy,
tel: +39 011 090 6845,
fax: +39 011 090 6899,
e-mail: marco.petrolo@polito.it

*Assistant Professor, e-mail: marco.petrolo@polito.it
†Ph.D. Student, e-mail: manish.nagaraj@polito.it
‡Ph.D. Student, e-mail: ibrahim.kaleel@polito.it
§Professor of Aerospace Structures and Aeroelasticity, e-mail: erasmo.carrera@polito.it

Abstract

A computationally efficient framework has been developed for the elastoplastic analysis of compact and thin-walled structures using a combination of global-local techniques and refined beam models. The theory of the Carrera Unified Formulation (CUF) and its application to physically nonlinear problems are discussed. Higher-order models derived using Taylor and Lagrange expansions have been used to model the structure, and the elastoplastic behavior is described by a von Mises constitutive model with isotropic work hardening. Comparisons are made between classical and higher-order models regarding the deformations in the nonlinear regime, which highlight the capabilities of the latter in accurately predicting the elastoplastic behavior. The concept of global-local analysis is introduced, and two versions are presented - the first where physical nonlinearity is considered for both the global and local analyses, and the second where nonlinearity is considered only for the local analysis. The second version results in reasonably accurate results compared to a full 3D finite element analysis, with a twofold reduction in the number of degrees of freedom.

Keywords: Elastoplasticity, global-local analysis, higher-order models, CUF

1 Introduction

Metallic structures are ubiquitous in various fields of engineering, and it is thus important to understand their mechanical behavior to optimize the design and predict failure. These structures typically undergo plastic deformation when loaded past the yield point, which necessitates a nonlinear analysis to determine the elastoplastic behavior. Numerical simulation is an important tool for such an analysis and is usually performed within the framework of the Finite Element Method. However, accurate stress fields are required when nonlinearities are involved, which often means that a 3D finite element analysis has to be performed. Such 3D simulations can be computationally very expensive, especially for the case of complex slender structures such as thin-walled beams. Significant efforts have therefore been exerted over the past few decades to find suitable alternatives to full 3D analysis. A starting point to achieve this is using analytical models, whereby intensive numerical computations can be avoided. An analytical formulation for inelastic beams was proposed by Timoshenko and Gere [1], whose validity was limited to doubly symmetric cross-sections and neglected shear deformations. An analytical solution to the elastoplastic bending of beams was reported by Štok, for the case of rectangular cross-sections [2]. The limitations of such models restrict their use as a general design tool. Numerical tools thus become essential for the nonlinear analysis of structures. Some of the simplest numerical approaches include the plastic hinge method where plasticity is assumed to be concentrated at a particular point [3], [4], [5].

A practical approach to numerically investigate elastoplastic behavior is to use 1D (beam) or 2D (plate/shell) finite elements, with enriched kinematics to better describe the deformation of the 3D structure. For instance, Prokić used warping functions to describe the out-of-plane deformations in thin-walled beams [6]. Some recent developments in FEM for thin-walled beams include the generalized beam theory (GBT), where cross-sectional deformation modes are computed to describe the deformed configuration. Elastoplasticity models developed using this formulation were successful in detecting localized plasticity and cross-sectional distortion in thin-walled structures without significant computational effort [7–10].

An approach to further reduce the computational cost associated with a nonlinear FE analysis is the use of global-local techniques. In general, such a procedure consists of the analysis of the coarsely meshed global structure, followed by the analysis over a finely discretized area of interest. The global solution is applied to the local domain as boundary conditions to drive the local analysis. Global-local techniques have frequently been used in the past decades for a refined linear structural analysis, when computing power was significantly expensive [11–14]. The use of such techniques to computationally intensive nonlinear analyses is a natural progression, leading to several researchers proposing various global-local methods to solve nonlinear problems. Noor applied the global-local methodology to investigate the nonlinear and post-buckling response of composite panels [15]. Duarte et al. developed a generalized finite element method based on global-local enrichment functions and applied it to investigate problems with confined plasticity [16, 17]. Gendre et al. presented a nonintrusive global-local technique for structural problems with local plasticity, using an iterative technique similar to [12], resulting in an exact structural re-analysis [18].

The objective of the current work is to predict the elastoplastic behavior of slender structures in a computationally efficient manner, by using a combination of the CUF and the global-local technique. In CUF, expansion functions are used across the beam cross-section to enrich the kinematics of the beam element, which results in 3D-like solutions at a reduced computational cost [19]. It, therefore, constitutes a suitable framework to perform nonlinear analyses. CUF has been recently extended to solve problems related to geometrical nonlinearity [20, 21], and physical nonlinearity [22]. The current work extends the previous work on elastoplasticity by incorporating global-local techniques within CUF to carry out a refined analysis in the plastic zone.

The paper is organized as follows: a brief overview of CUF is given in Section 2. The concept of global-local analysis and its implementation in the CUF framework has been explained in Section 3. Some numerical results have been presented in Section 4 to validate and demonstrate the capabilities of CUF in performing nonlinear analyses. Conclusions are drawn and presented in Section 5. The Appendix provides further details on the nonlinear implementation.

2 The Carrera Unified Formulation

The CUF is a unified framework which can be used to develop refined beam and shell/plate elements based on advanced structural theories. It uses expansion functions, F_τ, to enhance the displacements field, and hence to improve the kinematics of the FE model. For instance, the displacement field of a beam model, as shown in Fig. 1 can be described in CUF:

$$\mathbf{u} = F_\tau(x,z)\mathbf{u}_\tau(y), \tau = 1,2,\dots M \tag{1}$$

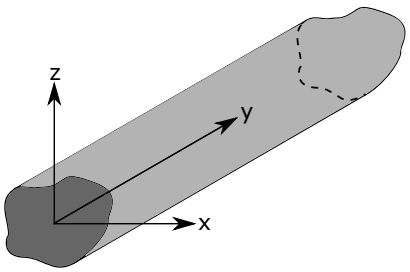

Figure 1: An arbitrary beam element aligned with the CUF Cartesian reference system

Where $F_\tau(x,z)$ is the expansion function across the cross-section, $\mathbf{u}_\tau$ is the generalized displacement vector, and M is the number of terms in the expansion function. The choice of F_τ and M are arbitrary and can be given as a user input. Two classes of expansion functions have been used for the current work, and are briefly described below.

Taylor Expansion (TE)

In this class of expansion functions, Taylor polynomials of the kind $x^i z^i$ are used as the expansion function F_τ, over the cross-section. The order of the polynomial is denoted by N and is specified by the user. As an example, the second-order TE (N = 2, TE2), containing 18 terms, is given below,

$$
\begin{aligned}
u_x &= u_{x_1} + xu_{x_2} + zu_{x_3} + x^2u_{x_4} + xzu_{x_5} + z^2u_{x_6} \\
u_y &= u_{y_1} + xu_{y_2} + zu_{y_3} + x^2u_{y_4} + xzu_{y_5} + z^2u_{y_6} \\
u_z &= u_{z_1} + xu_{z_2} + zu_{z_3} + x^2u_{z_4} + xzu_{z_5} + z^2u_{z_6}
\end{aligned} \tag{2}
$$

Classical beam theories such as Euler-Bernoulli Beam Theory (EBBT) and Timoshenko Beam Theory (TBT) can be obtained as special cases of the TE. In such a formulation, the unknown degrees of freedom are the displacements and their derivatives until the N^{th} order. A detailed explanation of the TE in CUF can be found in [23].

Lagrange Expansion (LE)

In this type of expansion, the cross-section is discretized using finite elements whose nodal interpolation functions are Lagrange polynomials. In such a formulation, the unknown degrees of freedom are purely the displacements in the spatial coordinates, and no rotations are involved. As an example, the displacement field of the 9-node bi-quadratic Lagrange element (L9) is given as

$$
\begin{aligned}
u_x &= \sum_{i=1}^{9} F_i(x,z) \cdot u_{x_i}(y) \\
u_y &= \sum_{i=1}^{9} F_i(x,z) \cdot u_{y_i}(y) \\
u_z &= \sum_{i=1}^{9} F_i(x,z) \cdot u_{z_i}(y)
\end{aligned} \tag{3}
$$

Where $u_{x_i}, u_{y_i}, u_{z_i}$ and F_i are the nodal translational degrees of freedom and Lagrange interpolation function of the i^{th} node, respectively. Multiple LE elements can be used to locally refined the displacement field. A detailed explanation of the LE in CUF can be found in [24].

Finite Element Formulation

The stress and strain tensors are represented in vector notation as follows:

$$
\begin{aligned}
\boldsymbol{\sigma} &= \{\sigma_{xx}, \sigma_{yy}, \sigma_{zz}, \sigma_{xy}, \sigma_{xz}, \sigma_{yz}\} \\
\boldsymbol{\varepsilon} &= \{\varepsilon_{xx}, \varepsilon_{yy}, \varepsilon_{zz}, \varepsilon_{xy}, \varepsilon_{xz}, \varepsilon_{yz}\}
\end{aligned} \tag{4}
$$

Where $\boldsymbol{\varepsilon}$ is the geometrically linear strain tensor. The linear strain-displacement relation is then given by

$$
\boldsymbol{\varepsilon} = \mathbf{D} \cdot \mathbf{u} \tag{5}
$$

Where $\mathbf{D}$ is the linear differentiation operator expressed as

$$\mathbf{D} = \begin{bmatrix} \frac{\partial}{\partial x} & 0 & 0 \\ 0 & \frac{\partial}{\partial y} & 0 \\ 0 & 0 & \frac{\partial}{\partial z} \\ \frac{\partial}{\partial y} & \frac{\partial}{\partial x} & 0 \\ \frac{\partial}{\partial z} & 0 & \frac{\partial}{\partial x} \\ 0 & \frac{\partial}{\partial z} & \frac{\partial}{\partial y} \end{bmatrix}$$

The elastoplastic stress-strain relation is given by

$$\boldsymbol{\sigma} = \mathbf{C}^{cep} : \boldsymbol{\varepsilon}^{e} \tag{6}$$

Where $\mathbf{C}^{cep}$ is the consistent elastoplastic tangent material matrix, and $\boldsymbol{\varepsilon}^{e}$ is the elastic component of the strain tensor $\boldsymbol{\varepsilon}$. Further details of the theory of elastoplasticity theory and its implementation in the form of the von Mises constitutive model has been given in the Appendix.

The beam is discretized along the axial direction with standard beam elements, using the nodal shape functions N_i, resulting in the following displacement field:

$$\mathbf{u}(x, y, z) = F_{\tau}(x, z) N_i(y) \mathbf{u}_{\tau i} \tag{7}$$

Based on the principle of virtual displacements,

$$\delta L_{int} = \delta L_{ext} \tag{8}$$

where δL_{int} is the virtual variation of the internal strain energy, and is given by

$$\delta L_{int} = \int_{V} \delta \boldsymbol{\varepsilon}^{T} : \boldsymbol{\sigma} \tag{9}$$

δL_{ext} is the virtual variation of the work due to external loading, and is denoted by

$$\delta L_{ext} = F_s N_j \delta \mathbf{u}_{sj}^{T} \mathbf{P} \tag{10}$$

where $\mathbf{P}$ is the external force vector. The virtual variation of the internal strain energy can be formulated using Eq. 6, 7 and 9, which results in the following equation for the stiffness matrix:

$$\delta L_{int} = \delta \mathbf{u}_{sj}^{T} \mathbf{k}_{ij\tau s}^{tan} \mathbf{u}_{\tau i} \tag{11}$$

where,

$$\mathbf{k}_{ij\tau s}^{tan} = \int_l \int_\Omega \mathbf{D}^T (N_i(y) F_\tau(x,z)) \mathbf{C}^{cep} \mathbf{D} (N_j(y) F_s(x,z)) \; d\Omega \; dl \tag{12}$$

The term $\mathbf{k}_{ij\tau s}^{tan}$ is the nonlinear Fundamental Nucleus (FN), and is a 3x3 matrix. Assembling the FNs calculated by looping through the indexes $\{i, j, \tau, s\}$ results in the element stiffness matrix. The reader is directed to [19] for a further understanding of the concept of the fundamental nucleus and its role in CUF.

3 Global-Local Analysis

The global-Local technique is used to analyze a complex structure in a computationally economical manner. Two distinct finite element models are considered in such a procedure: a coarsely discretized global model representing the entire structure, and a finely discretized local model representing the area of interest within the global structure. These regions are generally stress concentrators such as holes, cut-outs, sharp angles, etc. The solution of the global model is used as an input to the analysis of the local model, either in the form of mechanical boundary conditions (forces are prescribed), or geometrical ones (displacements are prescribed). These boundary conditions are prescribed at the interface between the local and global regions. A refined analysis can thus be carried out over the region of interest without requiring a fine discretization over the entire structure. It is noted that the global and local analyses are distinct from each other, resulting in a 2-step procedure that occurs sequentially. A schematic representation of a general global-local technique has been shown in Fig. 2. In the figure, part (a) represents the physical structure with applied boundary conditions. Part (b) of the figure shows the coarsely meshed global model with the local region (area of interest) highlighted. The finely meshed local model is shown in part (c).

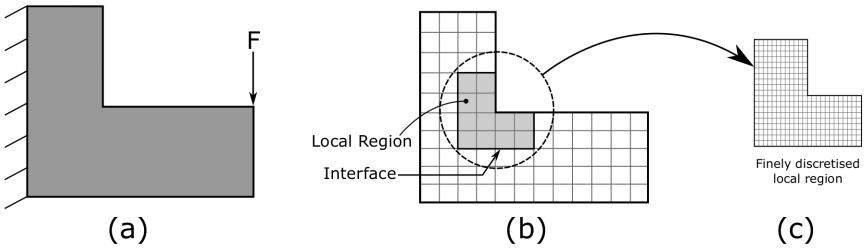

Figure 2: A schematic representation of the general global-local analysis procedure. (a) Physical structure with the applied boundary conditions, (b) the coarsely discretized global model, and (c) the finely discretized local region.

In the current work, the finite element model for the local region has been developed and analyzed in the CUF framework. A schematic representation of the global-local procedure in CUF has been shown in Fig. 3. The refinement is thus based on higher-order models, as opposed to using a very fine mesh. The 1D CUF model (for the local region) makes use of LE across the cross-section, since such an expansion has pure displacement unknowns, without involving higher-order derivatives as DOFs. Due to this, nodal displacements from the (coarse) global 3D mesh can be directly prescribed on to the local CUF model, as shown in Fig. 3, without the

need for ad hoc transformations of the global solution.

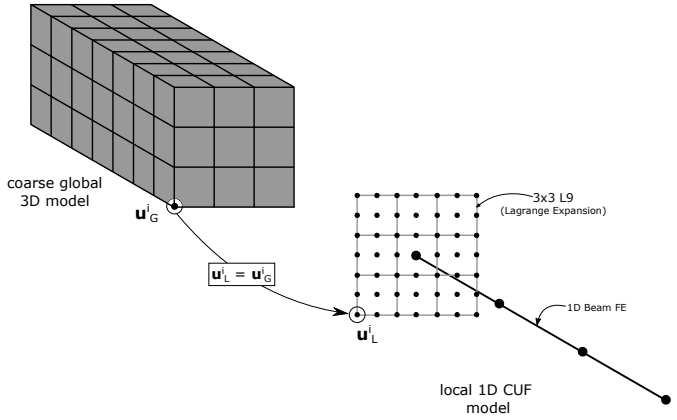

Figure 3: A schematic representation of the application of global displacements as boundary conditions on the CUF local model

Two variants of the global-local procedure have been presented, and are as follows:

1. Nonlinear Global - Nonlinear Local Analysis: In this case, a (physical) nonlinear analysis is carried out on the global model, and the results are used as boundary conditions in a (physical) nonlinear analysis of the local model. The global analysis is performed using a commercial software, ABAQUS, while the local analysis is done in CUF.

2. Linear Elastic Global Analysis - Nonlinear Local Analysis: In this case, a linear-elastic analysis is carried out on the global model, while a (physical) nonlinear analysis is performed on the local model. Both analyses are performed in the framework of CUF.

The use of ABAQUS in the first variant of the global-local procedure is to demonstrate the capability of CUF in interfacing with commercial FEA software. The objective of the second version listed above is to avoid nonlinear analyses wherever possible, and hence to reduce the amount of computational effort.

4 Numerical Examples

4.1 Cantilever beam under pure bending

This example serves to showcase the capabilities of the current implementation of the von Mises model in CUF. The structure is a cantilever beam with a square cross-section, clamped at one end and subjected to a prescribed displacement at the free end. A schematic representation of the structure is shown in Fig. 4. An isotropic material, i.e. steel, was considered with the following material properties: Young's Modulus E = 210.0 GPa, Poisson's ratio $\nu = 0.3$, and the yield stress $\sigma_{y0} = 210.0$ MPa. Perfect plasticity was assumed, resulting in a hardening modulus H = 0. The prescribed displacement at the free tip is u_z = -0.1 m.

The structure was analyzed in the framework of CUF using classical theories such as EBBT and TBT, as well as higher-order models based on TE and LE. Two cross-section discretizations were considered for the case

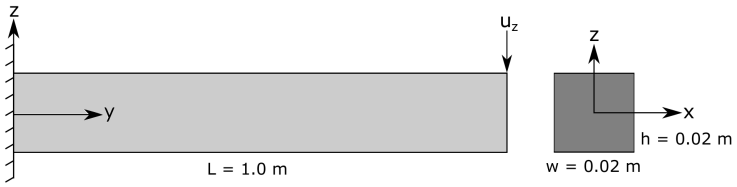

Figure 4: A schematic representation of the cantilever beam with the applied boundary conditions

of LE: 4L9 and 9L9, resulting in a 2x2 and 3x3 expansion element configuration respectively. A full 3D analysis was performed in ABAQUS, which serves to validate the results of the current work. The equilibrium path calculated according to various beam theories is plotted in Fig. 5. The vertical displacement u_z at the point x = 0.0, z = 0.0 and along the beam axis is plotted in Fig. 6. The axial stress σ_{yy} through the thickness of the beam at x = 0.0, y = 0.016 m, i.e., the center of the plastic region, is plotted in Fig. 7. A summary of the above analyses is presented in Table 1, which shows the vertical displacements at the point [x = 0.0, y = L/2, z = 0.0] as determined by various structural theories, along with the corresponding computational cost regarding the DOFs. Based on the above results, the following comments can be made:

1. Classical theories such as EBBT and TBT are unable to accurately capture the behavior of the structure as the material goes into the plastic regime. On the other hand, higher-order theories based on TE and LE can give better predictions of the nonlinear behavior. In fact, the axial stress along the cross-section presents a local nonlinear distribution that cannot be retrieved by low order models. This is consistent with the results reported by [22].

2. The use of higher-order elements within the framework of CUF leads to results which are in close agreements with a full 3D FEM solutions, yet requires over two orders of magnitude fewer DOFs. Such a physically nonlinear framework is thus very computationally efficient when compared to traditional solid FEA.

3. The use of TE (of order N) implies that a N^{th} order polynomial is used as the interpolation function across the entire cross-section. On the other hand, the Lagrange polynomials used in LE interpolate only across the domain of the particular expansion element. Better accuracy can, therefore, be obtained by the use of LE, due to the possibility of locally refining the cross-section discretization by the addition of Lagrange elements. This can be seen in Fig. 7, where the use of 9L9 elements gives better results than either 4L9 elements or TE (N = 3).

4.2 Bimetallic cantilever beam

The next example is similar to the previous case, with the exception that the beam is now multi-layered, with different material properties assigned to each layer. The upper half of the beam is made of aluminum, while the lower half is made of steel. A schematic representation of the structure is shown in Fig. 8 and the material

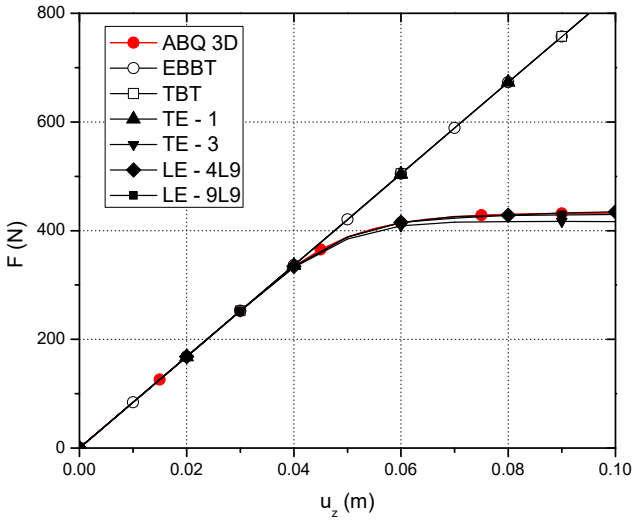

Figure 5: Equilibrium path of the cantilever beam according to various beam models

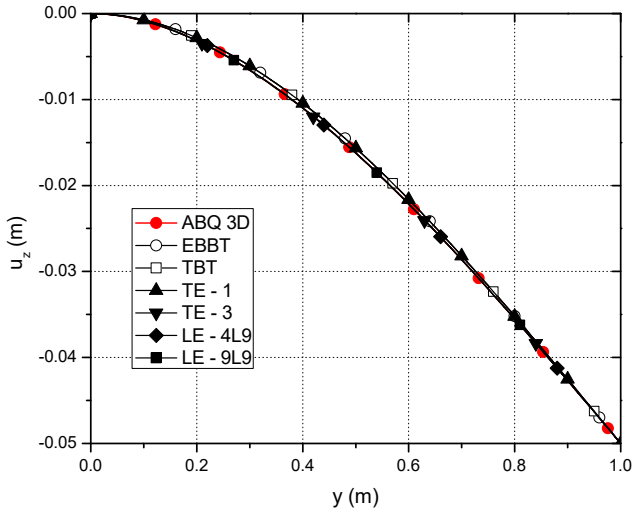

Figure 6: Vertical displacement u_z along the axis of the cantilever beam, at x = 0.0, z = 0.0, $u_z = -0.05\ m$

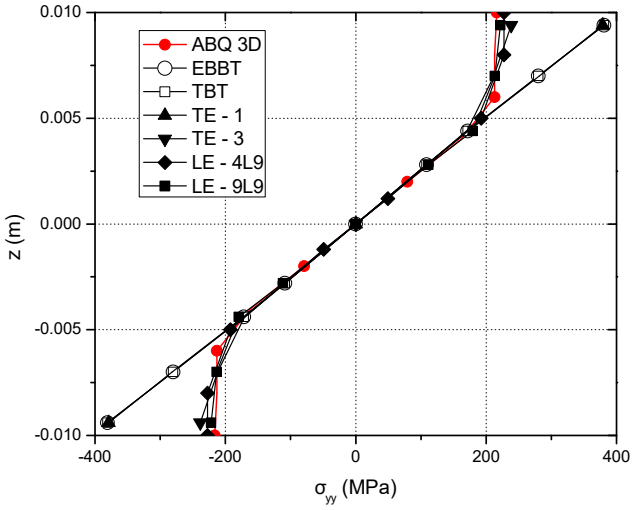

Figure 7: Axial stress σ_{yy} through the thickness of the cantilever beam, at x = 0.0, y = 0.016, $u_z = -0.05\ m$

	DOF	u_z (mm)
Reference		
ABAQUS - 3D Brick	694,023	-16.21
Current Analysis - CUF		
10 B4		
LE - 4 L9	2325	-16.09
LE - 9 L9	4557	-16.06
20 B4		
LE - 4 L9	4575	-16.17
LE - 9 L9	8967	-16.18
30 B4		
LE - 4 L9	6825	-16.18
LE - 9 L9	13,377	-16.20
40 B4		
EBBT	363	-15.64
TBT	605	-15.64
TE - 1	1089	-15.65
TE - 3	3630	-16.27
LE - 4 L9	9075	-16.21
LE - 9 L9	17,787	-16.21

Table 1: Vertical displacements u_z at the point (0.0, 0.5, 0.0) of the cantilever beam, as calculated by various structural theories, $u_z = -0.05\ m$

properties are listed in Table 2. Perfect plasticity was assumed for both materials, resulting in a hardening modulus H = 0.

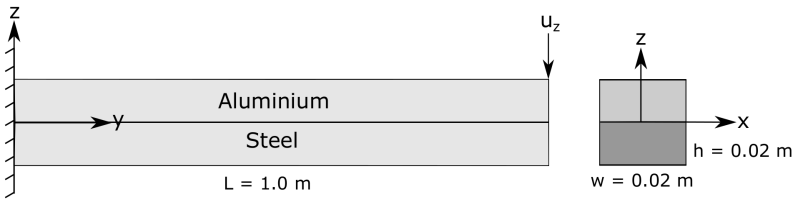

Figure 8: A schematic representation of the bimetallic cantilever beam with the applied boundary conditions

Property	**Aluminium**	**Steel**
Young's Modulus E	70.0 GPa	210.0 GPa
Poisson's Ratio ν	0.3	0.3
Initial yield stress σ_{y0}	110.0 MPa	210.0 MPa

Table 2: Material properties considered for the bimetallic cantilever beam

As before, the numerical analysis was performed using various structural theories within the framework of CUF, along with a full 3D analysis in ABAQUS for validation. The results of the numerical analyses shown hereinafter correspond to the application of 50% of the prescribed displacements, at which point the structure is well into the plastic regime. The vertical displacement u_z at x = 0.0, z = 0.0 and along the beam axis is plotted in Fig. 9. The axial stress σ_{yy} along the axis and at the top and bottom surfaces of the beam are plotted in Fig. 10. The axial stress through the thickness of the beam at x = 0.0 and y = 0.025 m, i.e., the center of the plastic zone, is plotted in Fig. 11. Table 3 summarizes the numerical results along with the computational costs regarding the DOFs. Some comments can be made based on the above results,

1. The presence of two material layers results in a complex stress distribution through the thickness of the beam. From Fig. 11, it can be clearly observed that the use of a refined cross-section mesh via 12 L9 elements leads to a very accurate solution, compared to a coarser 4 L9 mesh, or the use of a third-order polynomial in the case of TE.

2. The use of low order models affect the accuracy of results globally, independently of the presence of plasticity.

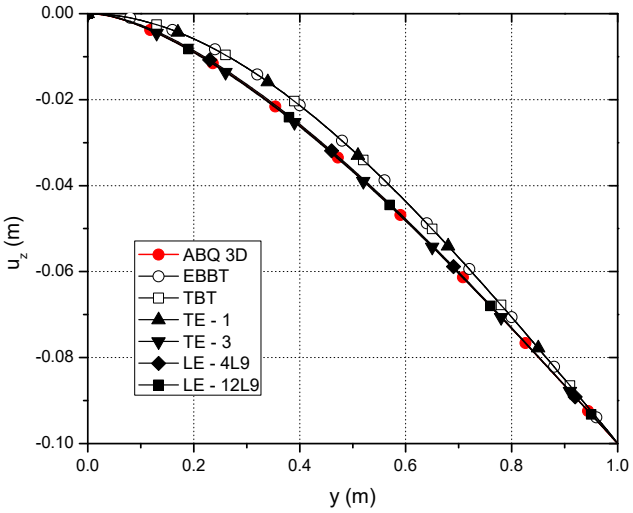

Figure 9: Vertical displacement along the axis (y) of the bimetallic cantilever beam at the point x = 0.0, z = 0.0

	DOF	u_z (mm)
Reference		
ABAQUS - 3D Brick	694,023	-36.56
CUF - 40B4		
EBBT	363	-31.79
TBT	605	-31.79
TE - 1	1089	-31.83
TE - 3	3630	-36.78
LE - 4L9	9075	-36.24
LE - 12L9	22,869	-36.57

Table 3: Vertical displacements u_z at the midspan of the bimetallic cantilever beam, as calculated by various structural theories

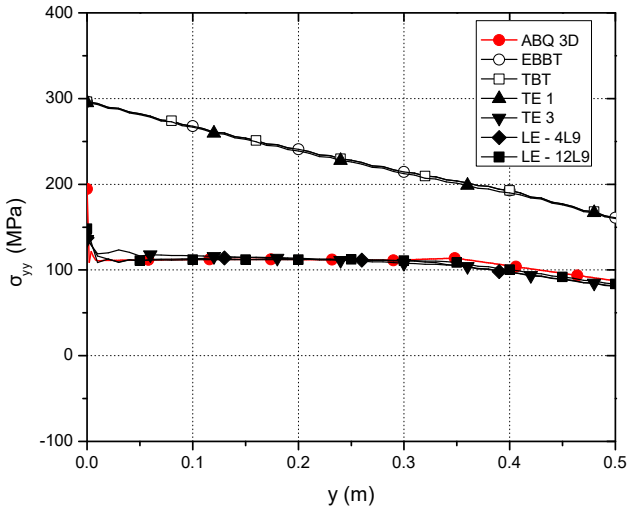

(a) At the top surface

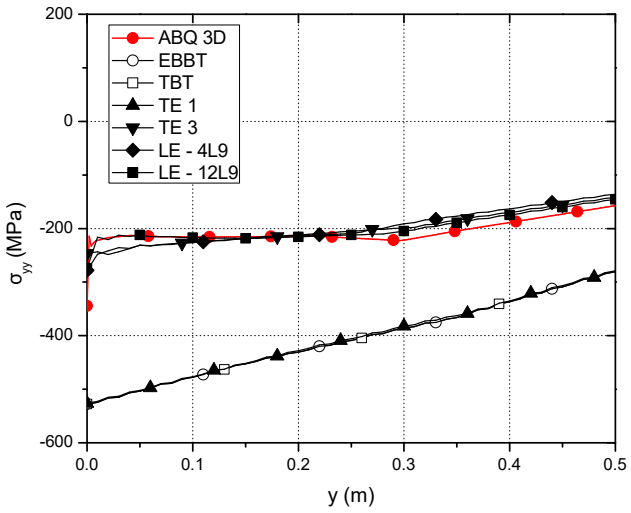

(b) At the bottom surface

Figure 10: Axial stress σ_{yy} along the axis of the bimetallic cantilever beam. (a) At the top surface (x = 0.0, z = 0.01), and (b) at the bottom surface (x = 0.0, z = -0.01)

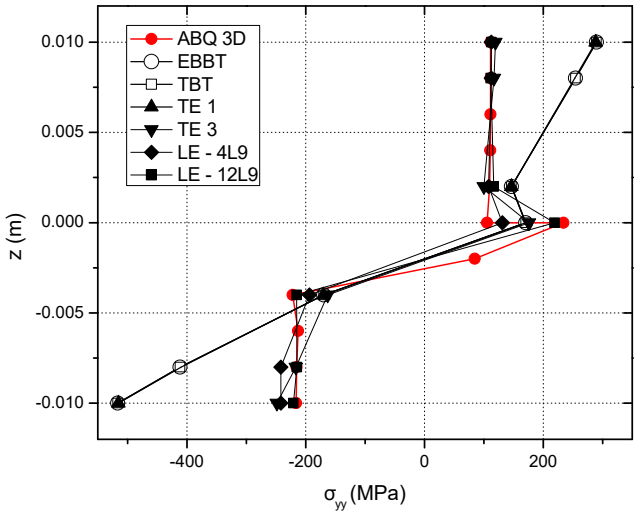

Figure 11: Axial stress σ_{yy} through the thickness (z) of the bimetallic cantilever beam, at the point x = 0.0, y = 0.025

4.3 Nonlinear Global - Nonlinear Local Analysis of a cantilever beam

The numerical example of 4.1 was considered once again for the current example, except that it is now analyzed using the technique of Global-Local Analysis. The geometry and material properties remain the same, and an initial analysis is performed in a commercial FEA software, ABAQUS, considering a coarse mesh with material nonlinearities enabled. This initial 'global' analysis serves to identify the plastic zone which can then be isolated as the local region, and also provides the displacement BC for the local region via the nodal displacements obtained as a result of the global analysis. The contour plot of the equivalent plastic strains as obtained by the global analysis is shown in Fig. 12, and the resulting local region is highlighted in the schematic representation of the full structure, as shown in Fig. 13.

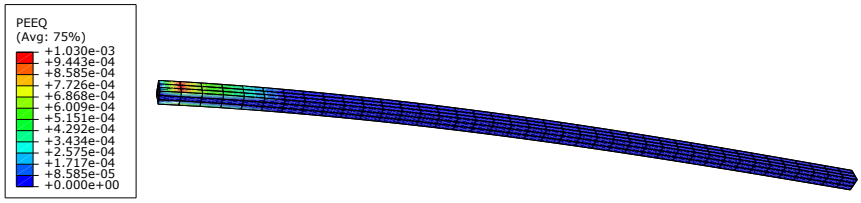

Figure 12: Contour plot of the equivalent plastic strain, obtained from the global analysis of the full structure

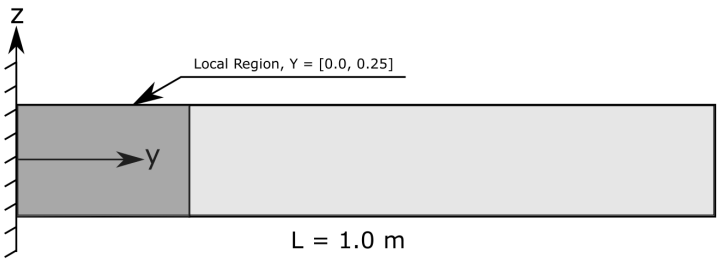

Figure 13: A schematic representation of the global cantilever beam with the local region highlighted

The results obtained using the global-local procedure were compared to those obtained using a monolithic analysis (based on various structural theories) over the entire global structure. All the results were validated via a refined mesh 3D analysis in ABAQUS. The vertical displacement u_z at x = 0.0, z = 0.0 and along the beam axis is plotted in Fig. 14, while the axial stress σ_{yy} through the thickness of the beam at x = 0.0, y = 0.016, which is the center of the plastic zone, is plotted in Fig. 15. Table 4 summarizes the results obtained via the different approaches, as well as the associated computational cost regarding the DOFs. Based on these results, a few comments can be made,

1. The global-local procedure provides results which are in close agreement with the reference 3D solution and requires fewer DOFs than either the ABAQUS 3D or the global CUF 1D models.

2. It can be seen in Table 4 that the global ABAQUS analysis over a coarse mesh fails to accurately predict the stress fields, while those obtained from the local CUF analysis (using a 20B4/9L9 discretization) are in close agreement with both the reference 3D and the global CUF (40B4/9L9) results. This motivates the use of a global-local procedure as a computationally efficient alternative to a monolithic global analysis (in either ABAQUS or CUF), which requires a highly refined mesh.

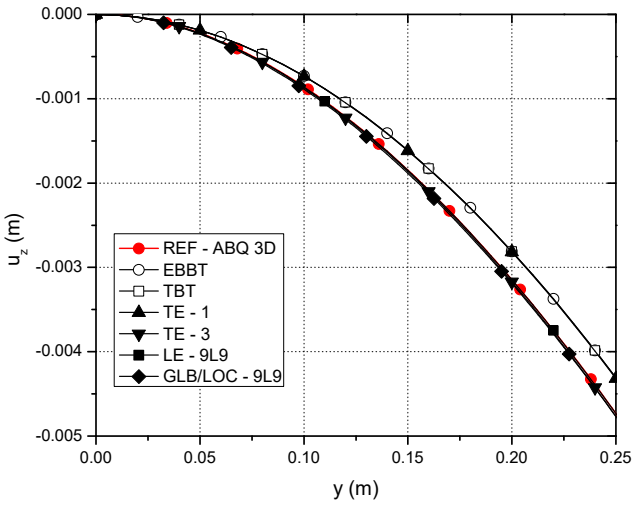

Figure 14: Vertical displacements along the axis of the local region, at the point x = 0.0, z = 0.0 (cantilever beam)

4.4 Nonlinear Global - Nonlinear Local Analysis of a Z-section beam

The current example was taken from [22] and is a suitable case to highlight the efficiency of global-local techniques in obtaining accurate 3D-like solutions at a reduced computational cost. The structure consists of a Z-section beam clamped at both ends and subjected to a pressure loading $p = 0.5\ MPa$ at the top and bottom flanges. A piece-wise linear hardening was considered by specifying a set of stress-strain points, which

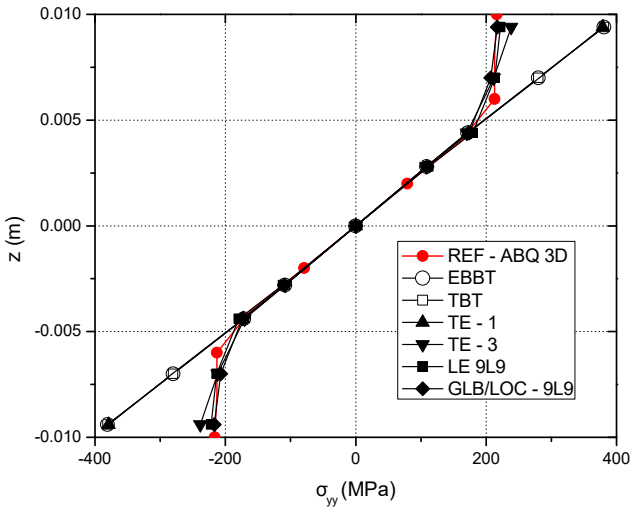

Figure 15: Axial stress through the thickness (z) of the beam in the local region, at the point x = 0.0, y = 0.016 (cantilever beam)

	DOF	u_z (mm)		σ_{yy} (MPa)
		y = 0.1	y = 0.5	x = 0.0, y = 0.1, z = 0.01
Reference				
ABAQUS - 3D Brick	694,023	-0.86	-16.21	214.4
CUF - 40B4				
EBBT	363	-0.73	-15.64	353.05
TBT	605	-0.73	-15.64	353.05
TE - 1	1089	-0.73	-15.65	352.68
TE - 3	3630	-0.87	-16.27	217.39
LE - 4L9	9075	-0.83	-16.21	215.59
LE - 9L9	17,787	-0.86	-16.21	216.3
Global-Local Analysis				
Global - ABAQUS	6840	-0.86	-16.25	236.6
Local - CUF (20B4/9L9)	8967	-0.89	–	216.1

Table 4: Numerical results calculated according to various structural theories and analysis strategies (cantilever beam)

are listed in Table 5. A schematic representation of the structure, along with the applied boundary conditions, is shown in Fig. 16. The figure also shows the 20L9 cross-section discretization used in the case of LE.

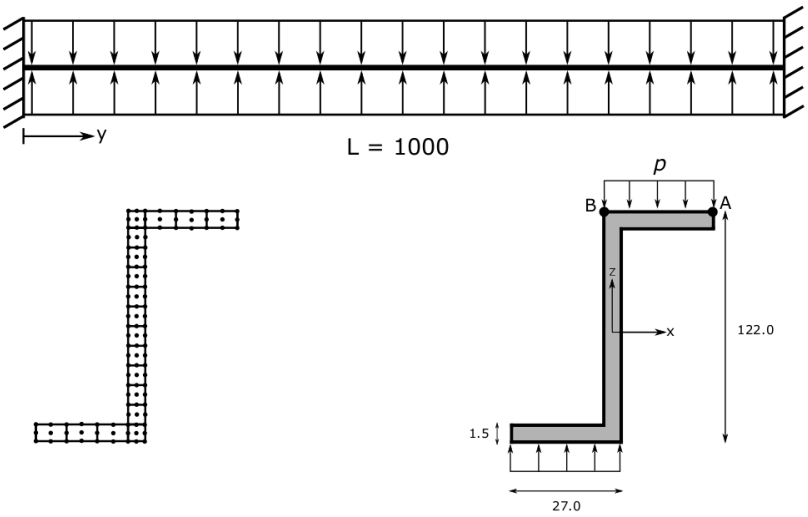

Figure 16: Schematic representation of the Z-section beam geometry, along with applied boundary conditions (dimensions in mm). The 20L9 cross-section discretization is illustrated.

Stress [MPa]	300	320	340	355	375	390	410	430	450	470	484
Plastic Strain	0.000	0.0002	0.00047	0.0012	0.0045	0.01036	0.0213	0.0344	0.0513	0.0800	0.147

Table 5: Piece-wise linear hardening data for the material used in the Z-section beam

An initial analysis (considering nonlinearities) was performed in ABAQUS 3D using a coarse mesh, to determine the plastic zone (area of interest) and hence to extract the nodal displacements at the boundary of this region, which would constitute the boundary conditions for the local analysis. A contour plot of the equivalent plastic strains is shown in Fig. 17, where the plastic zone can be clearly observed. Due to the symmetry of the structure, only one end of the beam is considered (where a plastic zone occurs) as the local region. Therefore, a segment of the beam corresponding to the range y = [0.0, 200.0] was considered for the local analysis.

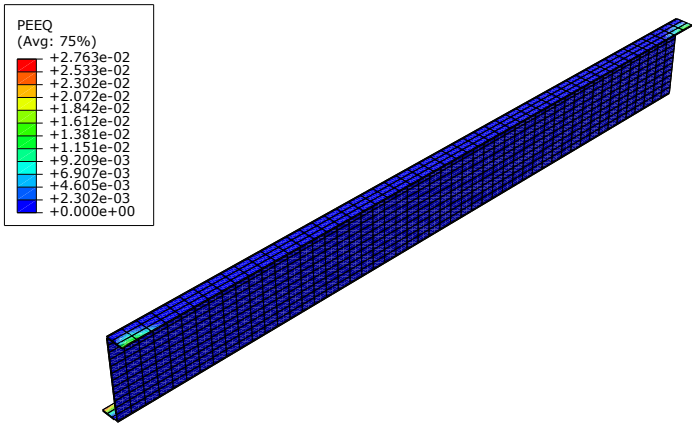

Figure 17: Contour plot of the equivalent plastic strains as reported by the initial global analysis in ABAQUS 3D

The results of the local analysis in CUF are shown along with a reference 3D solution obtained from ABAQUS, as well as a global solution obtained from CUF. It is noted that the same number of finite elements (20B4) and expansion elements (20L9) were used in both the CUF local model and the CUF global model (which is solely used for comparison). In the current case, only CUF structural theories considering an LE were considered. The displacement component u_x at the point A [x = 13.5, z = 61.0], plotted along the span of the local region, is shown in Fig. 18. The axial stress at the point B [x = -0.75, z = 61.0] along the local region axis is plotted in Fig. 19. A summary of the analyses comparing the numerical results and the computational costs is given in Table 6. Some comments can be made based on the above results,

1. The global-local approach results in a more accurate solution over the domain of the plastic zone when compared to a full CUF analysis, the number of DOFs remaining same. In both cases, the CUF analyses require one order of magnitude fewer DOFs than that required for the full 3D finite element analysis.

2. CUF beam models are capable of handling thin-walled beams, and of accurately identifying the plastic zones within the structure. This is consistent with the results of [22].

3. Performing a nonlinear analysis of the local model based on input from a nonlinear global analysis leads to a solution which is in good agreement with that of the reference 3D fine mesh analysis.

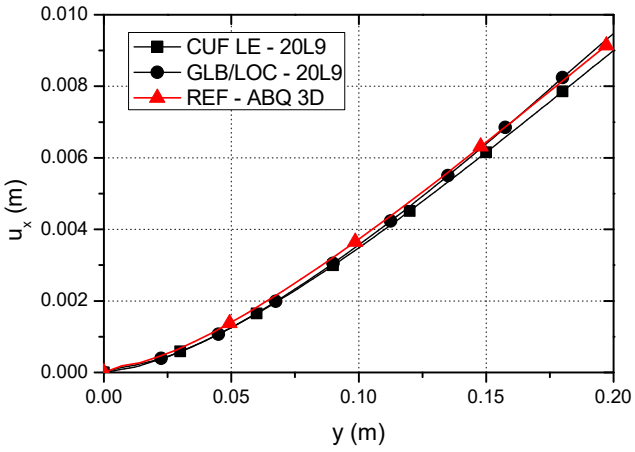

Figure 18: Horizontal displacement u_x at point A, along the span of the local region (Z-section beam)

	DOF	u_x (mm)
Global ABAQUS 3D	697,392	6.43
Global CUF - 20B4/20L9	22509	6.15
Global-Local Analysis		
Global - ABAQUS	22059	6.29
Local CUF - 20B4/20L9	22509	6.39

Table 6: Comparison of the horizontal displacements u_x at the point A and y = 0.1 m, determined using global analyses in CUF and ABAQUS, as well as the global-local technique (Z-section beam)

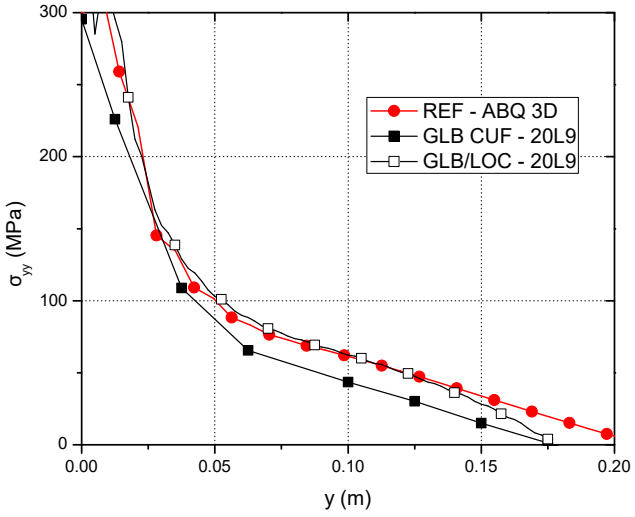

Figure 19: Axial stress σ_{yy} at point B, along the span of the local region (Z-section beam)

4.5 Linear Global - Nonlinear Local Analysis of a cantilever beam

This variation of the global-local procedure involves carrying out a linear elastic analysis over the global structure and using the linear global solutions as the boundary conditions for a local, nonlinear, analysis. Such a process is motivated by the fact that there exist certain cases where the nonlinearity is localized to a small zone within the global structure and does not significantly affect the global response. In such cases, the use of linear global solutions as boundary conditions does not cause remarkable changes to the stress fields in the local analysis. In the current example, the linear global - nonlinear local analysis was carried out in the framework of CUF, unlike the previous version of global-local analysis, where the global analysis was performed in ABAQUS and was nonlinear.

The cantilever beam of Section 4.1 was considered for the current analysis procedure. The extent of the plastic zone was determined by examining the magnitude of the von Mises stress σ_{vm} as reported by the linear global analysis. This can be easily done by introducing a parameter termed as the 'plasticity index', P_I, which is defined as the ratio of the von Mises stress to the initial yield stress, σ_{y0}, as given by the equation:

$$P_I = \frac{\sigma_{vm}}{\sigma_{y0}} \tag{13}$$

In the current example of the cantilever beam under pure bending, the maximum stresses occur at the top and bottom surfaces of the beam, and it is thus reasonable to expect the plastic zone to initiate at these surfaces, near the root of the beam. Therefore, the von Mises stress at the top surface of the beam (x = 0.0, z = 0.01) was considered for the computation of the plasticity index according to Eq.13, and is shown in Fig. 20. As can be seen from the figure, the index $P_I \geq 1$ for the range y = [0.0, 0.36]. This determines the approximate extent of the plastic zone, and hence the local region was considered to be the span extending till y = 0.4 m.

In general, the plasticity index can be computed for the entire structure and visualized using contour plots to determine the nonlinear zones, when the region of maximum stresses in the structure is not obvious.

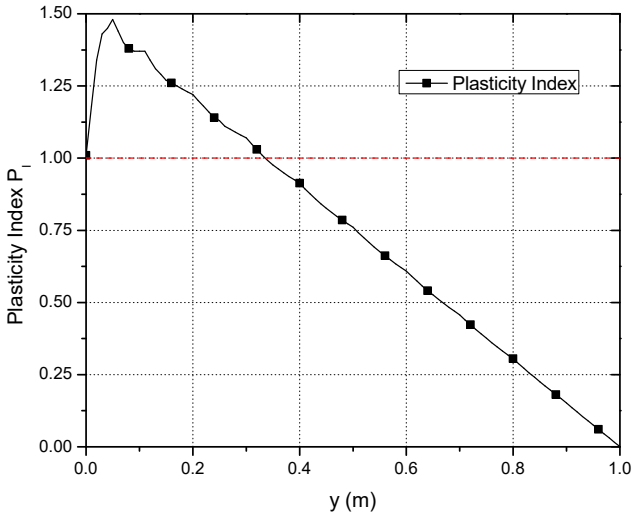

Figure 20: Plasticity index calculated along the length of the global model, at x = 0.0, z = 0.01

The nonlinear analysis of the local region was performed using 20B4 elements along the beam axis and 9L9 across the cross-section. The results of the local analysis are shown along with those of global CUF analyses (both linear elastic and with plasticity), along with a reference 3D nonlinear solution obtained using ABAQUS. The suffixes (EL) and (PL) indicate a linear elastic and nonlinear analysis, respectively. The vertical displacement u_z at the point x = 0.0, z = 0.0 and along the beam axis is plotted in Fig. 21. The axial stress σ_{yy} along the axis at the point x = 0.0, z = 0.01 is plotted in Fig. 22. The corresponding value through the thickness of the beam at the point x = 0.0, y = 0.016, which is the center of the plastic zone, is plotted in Fig. 23. The results of the numerical analyses along with the computational costs are given in Table 7. Some observations can be made based on the above results:

1. Using the solution of a linear elastic global analysis as boundary conditions for a nonlinear local analysis is sufficient to obtain reasonably accurate displacement profiles and stress fields in the local region corresponding to the plastic zone. This is an important observation since the inference is that the nonlinear analysis needs to be performed only in the required region, with a significant reduction of computational cost.

2. The global-local technique requires fewer DOFs than a monolithic CUF analysis, for the same accuracy in the results.

3. It can be seen that the local solution differs from the reference solution near the global-local interface. This is because linear elastic displacements were imposed on the interface. One way of solving this issue could be through an iterative approach where the nonlinear local results are inserted back into the linear

global analysis until convergence is achieved.

4. The plasticity index, P_I, is a suitable parameter to identify the plastic zone from the linear elastic global solution and can be useful in minimizing the domain of the nonlinear problem, making the overall analysis computationally efficient.

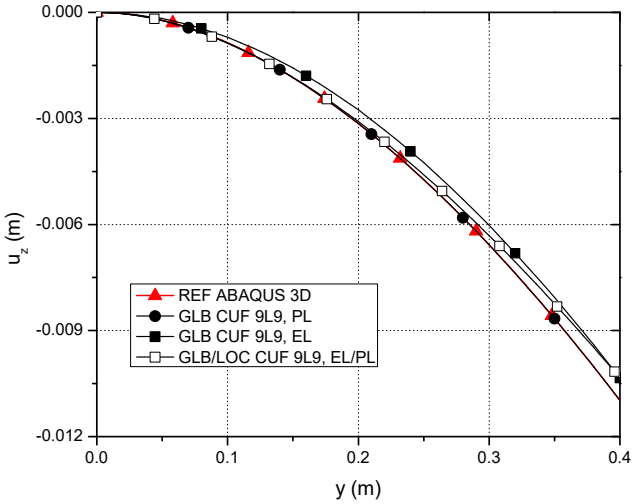

Figure 21: Vertical displacement u_z along the axis of the local region, at x = 0.0, z = 0.0 (cantilever beam)

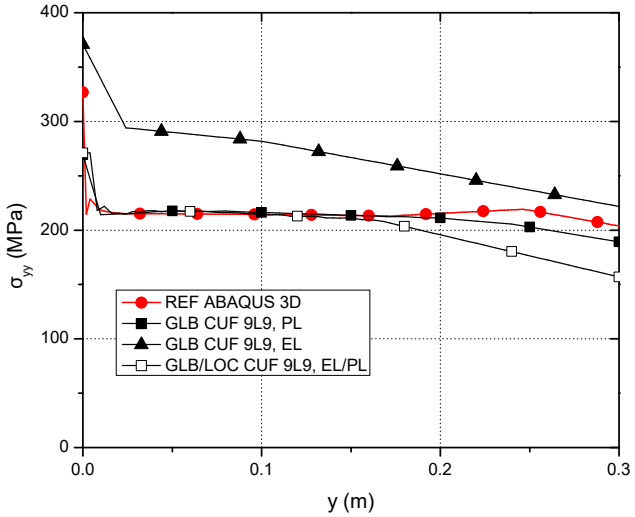

Figure 22: Axial stress σ_{yy} along the axis of the local region, at x = 0.0, z = 0.01 (cantilever beam)

5 Conclusion

A computationally efficient framework has been developed to solve problems of elastoplasticity in metallic structures, by a combination of global-local techniques and refined structural models available in CUF. The von

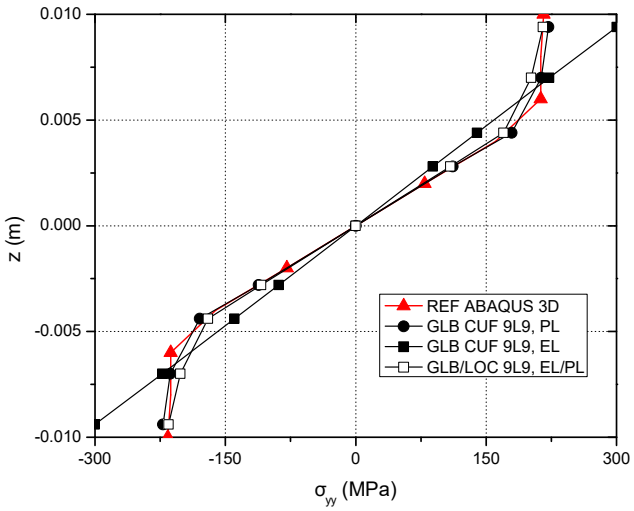

Figure 23: Axial stress σ_{yy} through the thickness of the local region, at x = 0.0, y = 0.016 (cantilever beam)

	DOF	u_z (mm)	σ_{yy} (MPa)
Global ABAQUS 3D (PL)	694,023	-0.86	214.4
Global CUF - 40B4/9L9 (PL)	17,787	-0.86	216.3
Global-Local Analysis			
Global CUF - 10B4/9L9 (EL)	4557	-0.70	265.48
Local CUF - 20B4/9L9 (PL)	8967	-0.87	214.9

Table 7: Summary of the numerical results obtained using a linear elastic global model and a nonlinear local model

Mises constitutive law was used within an incremental finite element framework to predict nonlinear behavior of compact and thin-walled beams in the plastic regime, restricting the problem to infinitesimal strain theory, i.e., assuming geometrical linearity. The numerical investigations were carried out using both classical and various types of higher-order beam theories, and the results were validated via a 3D analysis in commercial software, ABAQUS. Two types of global-local techniques were presented, where – (a) both the global and local analyses are nonlinear, and (b) the global analysis is linear elastic, while the refined local analysis is nonlinear. The aim of the latter version of the global-local technique is to minimize the region of the structure where a computationally intensive nonlinear analysis is carried out. The local region, i.e., the plastic zone, is identified by defining a parameter termed the Plasticity Index P_I. The results show that

1. Twofold reductions of the degrees of freedom are achievable compared to solid elements.

2. The use of a global linear solution does not affect the accuracy of the results significantly as soon as the plastic zone is limited in space.

3. The use of refined models is mandatory to capture the locally nonlinear distributions of stress along the cross-section due to plasticity and inhomogeneous material characteristics.

Future works shall include geometric nonlinearities and variable kinematics models to improve the computational efficiency of the analysis.

Acknowledgments

This research work has been carried out within the project ICONIC (Improving the crashworthiness of composite transportation structures), funded by the European Union Horizon 2020 Research and Innovation program under the Marie Skłodowska-Curie Grant agreement No. 721256, and the project FULLCOMP (Fully integrated analysis, design, manufacturing and health-monitoring of composite structures), funded by the European Union Horizon 2020 Research and Innovation program under the Marie Skłodowska-Curie Grant agreement No. 642121.

References

[1] S.P. Timoshenko and J.M. Gere. *Mechanics of Materials*. Springer, 1991.

[2] B. Štok and M. Halilovič. Analytical solutions in elasto-plastic bending of beams with rectangular cross section. *Applied Mathematical Modelling*, 33(3):1749–1760, 2009.

[3] J.G. Orbison, W. McGuire, and J.F. Abel. Yield surface applications in nonlinear steel frame analysis. *Computer Methods in Applied Mechanics and Engineering*, 33(1-3):557–573, 1982.

[4] G. Shi and S.N. Atluri. Elasto-plastic large deformation analysis of space-frames: A plastic-hinge and stress-based explicit derivation of tangent stiffnesses. *International Journal for Numerical Methods in Engineering*, 26(3):589–615, 1988.

[5] J.Y.R. Liew, D.W. White, and W. Chen. Second-order refined plastic-hinge analysis for frame design. part i. *Journal of Structural Engineering*, 119(11):3196–3216, 1993.

[6] A. Prokić. Material nonlinear analysis of thin-walled beams. *Journal of Structural Engineering*, 120(10):2840–2852, 1994.

[7] R. Gonçalves and D. Camotim. Generalised beam theory-based finite elements for elastoplastic thin-walled metal members. *Thin-Walled Structures*, 49(10):1237–1245, 2011.

[8] R. Gonçalves and D. Camotim. Geometrically non-linear generalised beam theory for elastoplastic thin-walled metal members. *Thin-walled structures*, 51:121–129, 2012.

[9] M. Abambres, D. Camotim, and N. Silvestre. Gbt-based first-order analysis of elastic-plastic thin-walled steel members exhibiting strain-hardening. *The IES Journal Part A: Civil & Structural Engineering*, 6(2):119–134, 2013.

[10] M. Abambres, D. Camotim, N. Silvestre, and K. Rasmussen. Gbt-based structural analysis of elastic–plastic thin-walled members. *Computers & Structures*, 136:1–23, 2014.

[11] K.M. Mao and C.T. Sun. A refined global-local finite element analysis method. *International journal for numerical methods in engineering*, 32(1):29–43, 1991.

[12] J.D. Whitcomb. Iterative global/local finite element analysis. *Computers & structures*, 40(4):1027–1031, 1991.

[13] J.D. Whitcomb and K. Woo. Application of iterative global/local finite-element analysis. part 1: Linear analysis. *International Journal for Numerical Methods in Biomedical Engineering*, 9(9):745–756, 1993.

[14] J.F.M. Wiggenraad and N.R. Bauld. Global/local interlaminar stress analysis of a grid-stiffened composite panel. *Journal of reinforced plastics and composites*, 12(2):237–253, 1993.

[15] A.K. Noor. Global-local methodologies and their application to nonlinear analysis. *Finite Elements in Analysis and Design*, 2(4):333–346, 1986.

[16] C.A. Duarte and D.J. Kim. Analysis and applications of a generalized finite element method with global–local enrichment functions. *Computer Methods in Applied Mechanics and Engineering*, 197(6):487–504, 2008.

[17] D.J. Kim, C.A. Duarte, and S.P. Proença. A generalized finite element method with global-local enrichment functions for confined plasticity problems. *Computational Mechanics*, 50(5):563–578, 2012.

[18] L. Gendre, O. Allix, P. Gosselet, and F. Comte. Non-intrusive and exact global/local techniques for structural problems with local plasticity. *Computational Mechanics*, 44(2):233–245, 2009.

[19] E. Carrera, M. Cinefra, M. Petrolo, and E. Zappino. *Finite element analysis of structures through unified formulation*. John Wiley & Sons, 2014.

[20] A. Pagani and E. Carrera. Unified formulation of geometrically nonlinear refined beam theories. *Mechanics of Advanced Materials and Structures*, 25(1):15–31, 2018.

[21] A. Pagani and E. Carrera. Large-deflection and post-buckling analyses of laminated composite beams by carrera unified formulation. *Composite Structures*, 170:40–52, 2017.

[22] E. Carrera, I. Kaleel, and M. Petrolo. Elastoplastic analysis of compact and thin-walled structures using classical and refined beam finite element models. *Mechanics of Advanced Materials and Structures*. In Press.

[23] E. Carrera and G. Giunta. Refined beam theories based on a unified formulation. *International Journal of Applied Mechanics*, 2(01):117–143, 2010.

[24] E. Carrera and M. Petrolo. Refined beam elements with only displacement variables and plate/shell capabilities. *Meccanica*, 47(3):537–556, 2012.

[25] E.A. de Souza Neto, D. Peric, and D.R.J. Owen. *Computational Methods for Plasticity: Theory and Applications*. Wiley, 2008.

Appendix

The von Mises model for elastoplasticity

This section elaborates on the nonlinear framework used in the present work. The implementation is based on [25], and a description of the various terms may be found in the appendix of [22]. The von Mises constitutive

law with linear isotropic hardening is described by the following set of equations:

$$\begin{aligned} \boldsymbol{\sigma} &= \mathbf{C} : \boldsymbol{\varepsilon}^e \\ f(\boldsymbol{\sigma}, \sigma_y) &= \sqrt{3J_2(\mathbf{S}(\boldsymbol{\sigma}))} - \sigma_y(\alpha) \\ \dot{\boldsymbol{\varepsilon}}^p &= \dot{\gamma}\mathbf{N} = \dot{\gamma}\frac{\partial f}{\partial \boldsymbol{\sigma}} \\ \alpha &= \dot{\bar{\boldsymbol{\varepsilon}}}^p = \sqrt{\frac{2}{3}}\|\dot{\boldsymbol{\varepsilon}}^p\| = \dot{\gamma} \end{aligned} \tag{14}$$

where $f(\boldsymbol{\sigma}, \sigma_y)$ is the yield function, $\mathbf{N} = \sqrt{\frac{3}{2}}\frac{\mathbf{S}}{\|\mathbf{S}\|}$ is the plastic flow vector and α is the hardening parameter. Eq. (A1.c) describes the associative flow rule used in the constitutive model.

The above set of differential equations is discretized using a Backward (implicit) Euler scheme, to obtain a set of algebraic difference equations. This can be used to formulate the discrete elastic predictor/plastic corrector two-step numerical algorithm based on the concept of return mapping, as shown in Fig 24. In this numerical scheme, given the solution at the time step t_n and the strain increment $\Delta\boldsymbol{\varepsilon}$, the solution at the next time increment t_{n+1} can be found by applying the following procedure:

1. Predictor - Elastic Trial Step

The trial strains are given by:

$$\begin{aligned} \boldsymbol{\varepsilon}^{e\ trial}_{n+1} &= \boldsymbol{\varepsilon}^e_n + \Delta\boldsymbol{\varepsilon} \\ \boldsymbol{\varepsilon}^{p\ trial}_{n+1} &= \boldsymbol{\varepsilon}^p_n \end{aligned} \tag{15}$$

The trial stresses can be calculated as:

$$\boldsymbol{\sigma}^{trial}_{n+1} = \mathbf{C} : \boldsymbol{\varepsilon}^{e\ trial}_{n+1} \tag{16}$$

The trial yield function, $f^{trial}_{n+1}(\boldsymbol{\sigma}^{trial}_{n+1})$, is calculated and the step is said to be elastic if it lies within the yield surface. The solution at t_{n+1} is then updated with the trial values. Plasticity occurs in the case when $f^{trial}_{n+1} \geq 0$, and the plastic corrector step is then initiated in the form of a return-map algorithm.

2. Corrector - The return map algorithm

The set of algebraic equations to be solved for the plastic case are:

$$\begin{aligned} \boldsymbol{\varepsilon}^e_{n+1} &= \boldsymbol{\varepsilon}^{e\ trial}_{n+1} - \Delta\gamma\sqrt{\frac{3}{2}}\frac{\mathbf{S}_{n+1}}{\|\mathbf{S}_{n+1}\|} \\ \alpha_{n+1} &= \alpha_n + \Delta\gamma \\ \sqrt{3J_2(\mathbf{S}_{n+1})} - \sigma_y(\alpha_{n+1}) &= 0 \end{aligned} \tag{17}$$

Eqs. 17 $(a-c)$ are in general nonlinear but can be reduced to a single nonlinear equation due to the cylindrical

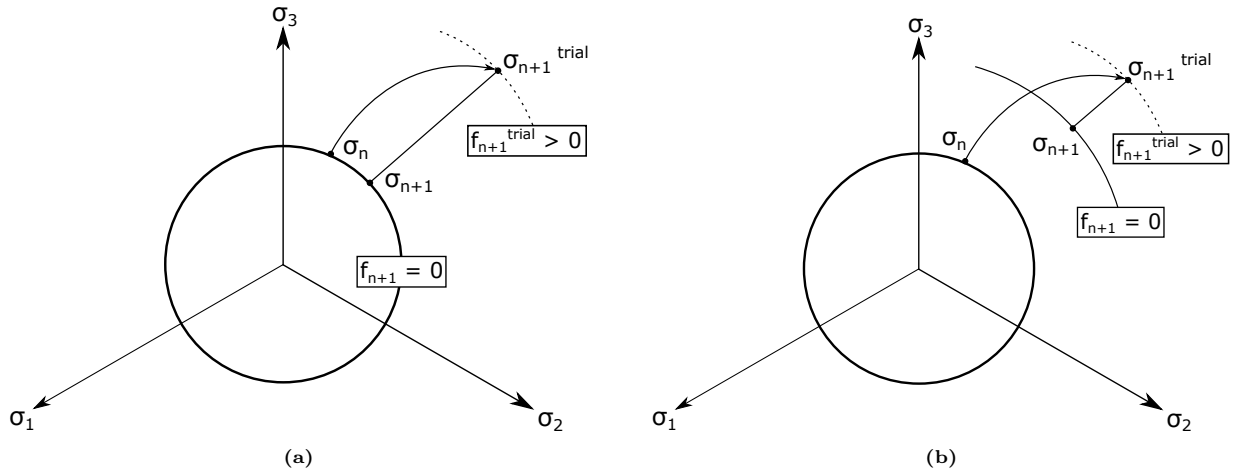

Figure 24: Return map algorithm for the von Mises constitutive model. (a) for the case of perfect plasticity, and (b) for the case of linear isotropic hardening.

nature of the von Mises yield surface, which results in a radial return mapping. The resulting equation is given by

$$\tilde{f}(\Delta\gamma) = q_{n+1}^{trial} - 3G\Delta\gamma - \sigma_y(\alpha_n + \Delta\gamma) = 0 \tag{18}$$

Where q_{n+1}^{trial} is the trial von Mises stress. Eq.18 can be solved using a second Newton-Raphson scheme for each iteration of the global Newton-Raphson loops, to compute the value of the plastic multiplier, $\Delta\gamma$. Once the incremental plastic multiplier has been determined, the stress and strain values can be updated as follows:

$$\begin{aligned}
\mathbf{S}_{n+1} &= \mathbf{S}_{n+1}^{trial}\left[1 - \frac{\Delta\gamma 3G}{q_{n+1}^{trial}}\right] \\
\boldsymbol{\sigma}_{n+1} &= \mathbf{S}_{n+1} + P_{n+1}^{trial}\mathbf{I} \\
\boldsymbol{\varepsilon}_{n+1}^{e} &= \frac{1}{2G}\mathbf{S}_{n+1} + \frac{1}{3}\boldsymbol{\varepsilon}_{v\ n+1}^{e\ trial}\mathbf{I} \\
\alpha_{n+1} &= \alpha_n + \Delta\gamma \\
\boldsymbol{\varepsilon}_{n+1}^{p} &= \boldsymbol{\varepsilon}_n^p + \Delta\gamma\sqrt{\frac{3}{2}}\frac{\mathbf{S}_{n+1}}{\|\mathbf{S}_{n+1}\|}
\end{aligned} \tag{19}$$

For the special case of linear isotropic hardening, Eq. 18 is linear, and hence an explicit form can be obtained for the solution of $\Delta\gamma$:

$$\Delta\gamma = \frac{f^{trial}}{3G + H} \tag{20}$$

In the current implementation of the model, a piece-wise linear hardening can be prescribed by providing a set of stress-strain points past the initial yield point, as shown in Fig. 25.

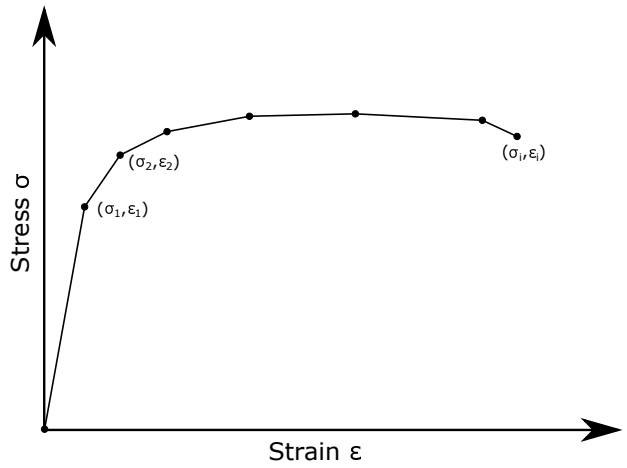

Figure 25: The stress-strain curve with piece-wise linear hardening, obtained by specifying a set of points

The consistent elastoplastic tangent operator

The consistent tangent elastoplastic operator is a fourth-order tensor that describes the elastoplastic nature of the material and relates the current values of stress and strain such that

$$\mathbf{C}^{cep} = \frac{\partial \boldsymbol{\sigma}_{n+1}}{\partial \boldsymbol{\varepsilon}_{n+1}} \tag{21}$$

The consistent tangent operator for the von Mises model with linear isotropic hardening is given as:

$$\mathbf{C}^{cep} = \mathbf{C} - \frac{\Delta\gamma 6G^2}{q_{n+1}^{trial}}\mathbf{I}_d + 6G^2\left[\frac{\Delta\gamma}{q_{n+1}^{trial}} - \frac{1}{3G+H}\right]\overline{\mathbf{N}}_{n+1} \otimes \overline{\mathbf{N}}_{n+1} \tag{22}$$

Where, $\mathbf{I}_d$ is the deviatoric projection tensor, $\mathbf{I}$ is the fourth-order identity tensor, and $\mathbf{C}$ is the linear elasticity tensor of fourth-order.

The term $\overline{\mathbf{N}}_{n+1}$ is defined as:

$$\overline{\mathbf{N}}_{n+1} = \sqrt{\frac{2}{3}}\mathbf{N}_{n+1} = \frac{\mathbf{S}_{n+1}^{trial}}{\|\mathbf{S}_{n+1}^{trial}\|} \tag{23}$$